Time-consistent estimation of LAI by assimilation in GreenLab plant growth model

Thomas Corpetti, Xing Gong, Mengzhen Kang, Baogang Hu, Laurence Hubert-Moy

Time-consistent estimation of LAI by assimilation in GreenLab plant growth model

Thomas Corpetti[1,2], Xing Gong[1,2], MengZhen Kang[1], BaoGang Hu[1], Laurence Hubert-Moy[2]

Abstract

This paper is concerned with the recovery of Leaf Area Index (LAI) time series in intense agriculture areas from moderate resolution remote sensing data (MODIS or SENTINEL). Although their resolution limits an analysis at a parcel level, their high temporal rate enables to monitor land use/land cover through the temporal evolution of key biophysical parameters as LAI. However in practice, frame-by-frame estimation is unsatisfactory since the quality of each single data is subjected to undesirable effects due to atmosphere disturbance, sun geometry, viewing geometry, etc. These effects lead to a lack of temporal consistency of resulting time series. The reconstruction of such time series is delicate using conventional interpolation methods since underlying physical processes are not taken into account. In this paper, we tackle this issue by exploiting the prior information of a plant growth model, namely GreenLab, using stochastic data assimilation techniques. Our experiments on challenging situations, such as few data and fragmented landscapes, demonstrate the approach is robust on various challenging situations and enables to extract additional information about observed fields. Experiments are performed on MODIS data.

Index Terms

Leaf Area Index, GreenLab model, data assimilation, noisy/missing data

[1]: CASIA : Chinese Academy of Sciences, Institute of Automation, LIAMA (Sino European Lab on Computer Sciences and Applied Mathematics), ZhongGuanCun East Road, Beijing 100190, China

[2]: CNRS : French National Center for Scientific Research & University of Rennes 2, Place du Recteur Henri Le Moal, 35043 Rennes Cedex, France

All authors have discussed together about methodological developments. Thomas Corpetti and Gong Xing implement code and make tests. MengZhen Kang and BaoGang Hu gave their skills in GreenLab model and Laurence Hubert-Moy gave her skills about applications on the study site

I. Introduction

A. Land surface monitoring

Land surface on earth is mainly covered by green plants including forests, grasslands or agricultural fields (Townshend *et al.* (1991)). These vegetation areas are of great importance for global ecological systems and food supply for human beings. Therefore in the past several decades, many satellites have been launched to observe and monitor these areas (Richards (2013); Trotter (1991)). A number of important tools has been developed to extract some crucial information on crops and plants from satellite images. This is indeed a prerequisite in many agricultural applications such as monitoring the plant physiology and/or ecology at different scales (Gao (1996); Huete (1988); Liang (2005)). One of the most popular vegetation index is the NDVI (Normalized Difference Vegetation Index, Rouse Jr *et al.* (1974)), based on the spectral reflectance property of green leaves (chlorophyll) at different spectral bands and computed using red and near-infrared wavebands. While NDVI is a sensitive indicator of canopy structure and chemical content (plant biomass, leaf area index, chlorophyll content in sparse canopies and foliar nitrogen content), it is still a limited index for total canopy biomass in high-density vegetation areas (Gamon *et al.* (1995)). Some other more sophisticated biophysical indexes have been proposed, such as :

- **fCover (vegetation cover fraction)**: which represents the fraction of ground covered by green vegetation;
- **fAPAR (fraction of photo-synthetically active radiation absorbed by the canopy)**: which represents the fraction of the solar radiation absorbed by live leaves;
- **LAI (Leaf Area Index)** : which represents the total quantity of green leaf area per unit ground surface area.

In practice, fAPAR is sensitive to sun lighting while fCover and LAI are independent from the illumination. In this study we rely on LAI since the total quantity of leaves is captured (and not only the ground surface); moreover, this parameter is largely used in practice (Baret *et al.* (2007)), for example to estimate productivity for certain crops. Readers can find in Carlson and Ripley (1997); Gamon *et al.* (1995) more details about these biophysical variables. The estimation of these biophysical variables from remote sensing is a delicate task. Several models, based on light interception by plant canopies and vegetation reflectance in terms of biophysical characteristics, have been designed and inverted to retrieve biophysical information

from optical satellite images. Among them, SAIL (Scattering by Arbitrary Inclined Leaves) canopy bidirectional reflectance model Verhoef (1984) and PROSECT (based on leaf optical properties) are widely used Schaepman-Strub *et al.* (2006). Even though the results were globally satisfactory, strong improvements have been obtained when one mixes these two models. The resulting one, PROSAIL, has allowed to describe both the spectral and directional variation of canopy reflectance based on single static images (Jacquemoud *et al.* (2009); Lecerf *et al.* (2008); González-Sanpedro *et al.* (2008)).

All these methods have been designed for single images and only few of them exploit the time series observation to derive the plant growth evolution information : in Roerink *et al.* (2000), authors have developed a Fourier analysis method to reconstruct cloud free NDVI composites while in Jonsson and Eklundh (2002), the authors have proposed a technique based on nonlinear least squares. Despite the fact that they provide interesting information, no physical knowledge about plant or vegetation growth is taken into consideration.

In this study we suggest to exploit the short revisit period of satellites to improve the quality of estimated biophysical variables by constraining the solution to be consistent with physical dynamic priors. This *data assimilation* procedure, though presented here for LAI estimation, can be applied to any biophysical variable provided that a physical model of its temporal evolution exists.

B. Plant growth modelling

The term *plant modelling* has various meanings depending on scientific communities. One can simulate realistic forms and patterns of plants from an architectural and geometrical point of view (Fisher (1992)), as in earlier developments (see for example Cohen (1967); Honda (1971); Lindenmayer (1968)). This *structural* simulation of plants refers to various tools either related to L-systems (Przemyslaw *et al.* (1988)), fractals (Smith (1984)), particle systems (Reeves and Blau (1985)) or ramified matrix (Viennot *et al.* (1989)) for example.

When one is concerned with more physical studies related to plants and crops (agronomy, forestry, biophysics, ...), specific plant growth models have been developed for agronomic purposes, harvest prediction or optimum crop management (see for an Brisson *et al.* (2003)) and rely on *physical* properties: they describe the flux of external and internal resources through the element “plant” in order to expect its yield. These *process-based models* (PBM) consider biomass

production through the photosynthetic process and the global biomass partitioning among organs (Heuvelink (1999) or Dayan *et al.* (2004)).

Between process-based models and architectural models, *functional-structural plant models (FSPM)* have emerged since the end of the 1990's (see De Reffye *et al.* (1997); Kurth and Sloboda (1997); Perttunen *et al.* (1996); Vos *et al.* (2007); Yan *et al.* (2004)). They perform efficient and realistic dynamic simulations of plant morphogenesis (see for example Jallas *et al.* (2000); Perttunen *et al.* (1996)) by taking into account both physical and structural properties. The GreenLab plant growth model (Yan *et al.* (2004)) belongs to this family and has been designed to provide dynamic representations of the morphogenesis and architecture of plants. Because of *i)* its efficiency in modelling realistic physical behaviours ; *ii*) its efficiency in designing consistent plant architectures and *iii)* its permanent interaction between structural and functional part, this model is really interesting for plant studies. We therefore rely on it in this paper.

C. Contributions and novelty of the paper

Though generating LAI by assimilating remote sensing data in crop model has already been studied (see for example Launay and Guerif (2005); Zhao *et al.* (2013); Dente *et al.* (2008); Curnel *et al.* (2011)), only a specific culture (sugar, maize, wheat) has been explored in most of these studies. In addition, associated models do not contain a functional part as GreenLab do, and this latter has never been used yet for data assimilation. This is the scope of this paper.

The overall article is organised as follows: the next section introduces the principles and required details of GreenLab plant growth model. As this model is designed at a plant level, some manipulations and simplifications are required for its adaptation to medium resolution images. These modifications, detailed in section II-B, enable to finally exploit an easy-to-use version for data assimilation. The assimilation part is presented in section II-C and finally, section III show some experiments on synthetic and real data.

II. Material and Methods

A. Introduction to the Greenlab model

GreenLab model aims at simulating plant growth evolution. For each type of plant, this model is calibrated with ad-hoc observations of growth made under controlled environment and where extensive and even destructive measurements of individual plants are made regularly Guo *et al.* (2006); Kang *et al.* (2008). This enables to derive a deterministic description of a plant evolution

(in more recent research, some stochasticity has been introduced to bring about plant growth variations Lopez *et al.* (2008); Wang *et al.* (2011)). The model works sequentially and in each cycle, two steps are performed:

1) **Biomass production:** this step generates a biomass pool from some environmental parameters (sun lighting, photosynthesis efficiency, plant density, ...);
2) **Biomass repartition:** the generated biomass is shared between some organs (leafs, fruits, ...).

The idea behind this model is that all organs of a plant share a common biomass pool and are therefore in competition each others. In addition to these two primal operations, a **natural withering** of each plant is modelled. This is schematised in figure 1 and main steps are detailed below.

1) Biomass production: The biomass production comes from a large number of factors as photosynthesis efficiency of plant species, total leaf area, environmental context, etc. In GreenLab, the production is done over growth cycle through the relation:

$$Q_{t_k} = E \cdot S_p \cdot \frac{1}{r}\left(1 - exp\left(-k \cdot \frac{S_{t_k}}{S_p}\right)\right) \tag{1}$$

where:

- Q_{t_k} is the Biomass generated at the growth cycle between t_k and t_{k+1} ;
- E is an empirical environmental factor (sun lighting, temperature, etc);
- S_p is the land occupation of the plant;
- k is photosynthesis efficiency;
- r is an resistance parameters, setting the effect of mutual shading;
- S_{t_k} is the total leaf area at t_k.

From Eq. (1), one observes that biomass generation is largely dependent of the leaf area S_{t_k} and is also restricted by land occupation S_p, surrounding environment E and species-dependent coefficient constant r, k.

This description is the one that will be used in our data assimilation process. Let us now describe the biomass repartition step.

2) Biomass repartition: Once the biomass is produced, it has to be redistributed among the different organs of the plant following their own demand. To this end, for each kind of organ o in the set of organs Ω (Ω can contain organs as leaves, branches, sheath tassel, cob, ... as will be seen later we will focus mainly on branches b, leaves ℓ and fruits f) one has to compute

its *biomass increment* $\Delta_{q_o}(t_{k+1})$ at time t_{k+1} following some rules described below (Yan *et al.* (2004)):

$$D_{t_{k+1}} = \sum_{o \in \Omega} \left(N_o(t_{k+1}) \sum_{t=1}^{t_{k+1}} d_o(t) \right) \tag{2}$$

$$d_o(t) = S_o \cdot \phi_o(t) \tag{3}$$

$$\Delta_{q_o}(t_{k+1}) = d_o(t_{k+1}) \cdot \frac{Q_{t_k}}{D_{t_{k+1}}} \tag{4}$$

with

- $D_{t_{k+1}}$ the total biomass demand in the beginning of cycle t_{k+1} depending on all organs $o \in \Omega$;
- $d_o(t)$ the biomass demand of an organ $o \in \Omega$ for time t;
- S_o the sink-strength of organ $o \in \Omega$;
- $\Delta_{q_o}(t_{k+1})$ the increment of biomass related to organ $o \in \Omega$ in the end of cycle cycle k;
- $N_o(t_{k+1})$ the active number of organ of type o at time t_{k+1};
- $\phi_o(t)$ a beta law function related to the demand of each organ. This latter is small at the beginning and end of organ growth and relatively large during the growth process Guo *et al.* (2006). It takes the following form:

$$\phi_o(t) = (t - 0.5)^{a_o - 1} \cdot (t_{go} - t + 0.5)^{b_o - 1} \tag{5}$$

  where a_o, b_o and t_{go} are parameters related to an organ. More precisely, t_{go} is called *expansion time* for organ o and indicates the growing period: after this step, it does not join the biomass repartition in Eq. (2) anymore (this models for example the fact that stalks stop to grow after autumn). Parameters a_o and b_o are calibration ones related to each organ.

As one can see, the association of the biomass to one specific organ is based on its demand d_o (cf Eq. (3)) and depends on its sink strength S_o and growth age. The strength is plant-dependent: for example concerning fruit trees, the fruit organ tends to have more demand than a tiny root. Therefore S_o in Eq. (3) is bigger for the fruit organ than tiny root one. As for the age component, GreenLab assumes that an organ grows relatively slowly at the beginning and end of his life and accumulate most portion of biomass in the middle part. This is modelled by function $\phi_o(t)$. Finally, the role of Eq. (4) is to distribute the biomass among organs based on individual demands and the total available biomass.

3) Natural withering: Regarding leaf area index S_{t_k} related to organ *leaf* (noted ℓ, which is the variable of interest in this paper) and without withering, a natural evolution model for S_{t_k} would be $S_{t_{k+1}} = S_{t_k} + \Delta_{q_\ell}(t_{k+1})$. To model the fact that each organ naturally dies after a given time, a withering of all plants is modelled through the following rule:

$$S_{t_{k+1}} = \alpha \cdot (S_{t_k} - \beta(t_k, t_{e\ell})) + \Delta_{q_\ell}(t_{k+1}). \tag{6}$$

This equation expresses the fact that in the end of cycle t_k, the next leaf area $S_{t_{k+1}}$ will be increased by $\Delta_{q_\ell}(t_{k+1})$, the growth of organ *leaf* issued from equation (4). This is altered by $(\alpha, \beta(t_k, t_{e\ell}))$. The rule of coefficient $\alpha \in [0, 1]$, which stands for the spoilage in natural growth, is to model a global withering while function $\beta(t_k, t_{e\ell})$ is time-varying and relies on the *life expectance* (roughly speaking the "birth") $t_{e\ell}$ of leaves ℓ. The value of this function will be discussed in next section.

Equations (1–6) are the core of the GreenLab model for biomass generation, partition and withering. This model is dependant from many parameters. It is useful to *simulate* plant growth from known parameters but obviously their *recovery* from image sequences appears impossible, as pointed out in Yang *et al.* (2008). Fortunately, many simplifications related to medium resolution remote sensing images are possible and we can design an assimilation tool based on GreenLab principles. This is the scope of next section.

B. Simplified Greenlab for remote sensing data assimilation

We suggest to simplify and adapt the initial GreenLab model to remote sensing. Though the biomass generation process does not change, all details regarding the internal structure of plants can be simplified. Associated manipulations are detailed bellow.

1) Focus main organs: We decide to take into consideration only the *three* most important organs responsible of the majority of biomass production: leaf, fruit and branch (internode), respectively noted (ℓ, f, b), yielding a set of organs $\Omega = \{\ell, f, b\}$, the remaining ones being modelled with noises, as will be shown in equation (10).

2) Plant structure simplification: In order to describe plant structure evolution, we keep an empirical *Look-Up-Table*, $U = \{U_i | i = 1, ..., N\}$ which store statistical number for different appearing organs. For instance, $U_4 = \{\ell = 3, b = 2, f = 0\}$ means that at 4_{th} growth cycle, there would be 3 new leaves, 2 new internodes and no new fruits (one also notes $U_4\{\ell\} = 3$, $U_4\{b\} = 2$ and so on). In practice, available Look-Up-Tables for more than 30 species are

already available (see for example Ma *et al.* (2006); Mathieu *et al.* (2007); Wang *et al.* (2009)) and are used in this study.

3) Natural withering modelling: In equation (6), the withering of leaves at the growth cycle between t_k and t_{k+1} is modelled with function as $\beta(t_k, t_{e\ell})$. This function is plant-dependent and is conditioned by the age of leaves which in practice is available through the structural sub-model. To prevent from the dependency from this age and on the kind of plants, we rely on the *active number of organs* $N_o(t_k)$ computed using the Look-Up-Tables U previously defined:

$$N_o(t_k) = \sum_{i=t_k-t_{eo}}^{t_k} U_i\{o\}. \tag{7}$$

where t_{eo} is the expectance-time for any organ $o \in \Omega$. Concerning function $\beta(t_k, t_{eo})$ in Eq. (6), its formulation is based on leaves's appearing time and life expectance t_{eo} as:

$$\beta(t_k, t_{eo}) = \frac{U_{t_k-t_{eo}}\{\ell\}}{N_\ell(t_k)} \cdot S_{t_k} \tag{8}$$

with N_ℓ the active number of leaves. Its expression is in practice computed using available Look-Up-Tables and relation (7).

4) Overall model used for data assimilation: To model potential errors likely to arise because of the three aforementioned kind of simplifications, a white gaussian noise of standard deviation η_{t_k} is introduced for each t_k. Therefore, the overall sequential model to compute Leaf Area Index $S_{t_{k+1}}$ based on S_{t_k} and greenlab reads:

$$S_{t_{k+1}} = \alpha \cdot (S_{t_k} - \beta(t_k, t_{eo})) + \Delta_{q_\ell}(t_{k+1}) + \eta_{t_k}. \tag{9}$$

Using relations (1) to (8), one can reformulate the above plant growth model by:

$$\begin{aligned} S_{t_{k+1}} &= M_k[S_{t_k}] + \eta_{t_k} \\ &\text{with:} \\ M_k[S_{t_k}] &= \underbrace{\alpha\left(1 - \frac{U_{t_k-t_{eo}}\{\ell\}}{N_\ell(t_k)}\right) S_{t_k} - \frac{ES_p d_o(t_{k+1})}{rD_{t_{k+1}}} \exp\left(-k \cdot \frac{S_{t_k}}{S_p}\right)}_{\text{non linear model w.r.t. } S_{t_k}} \\ &+ \underbrace{\frac{ES_p d_o(t_{k+1})}{rD_{t_{k+1}}}}_{\text{independent from } S_{t_k}} \end{aligned} \tag{10}$$

where the *unknown parameters* to recover are:

- S_{t_k} the Leaf Area Index at time t_k ;

- k the photosynthesis efficiency parameter in equation (1);
- E/r a coefficient related to the external influence (environmental over resistance parameter) in equation (1);
- α standing for the spoilage in natural growth in equation (6);
- t_{el} standing for the life expectance of leaves;
- η standing for the noise due to model errors in equation (10).

All other parameters involved in (10) are available through Loop-Up-Tables and from relations (2) to (5). The second term of $M_k[S_{t_k}]$ in (10) does not depend on the variable of interest S_{t_k} and the first one is nonlinear because of its exponential part. This model will be used in our assimilation process.

In Figure 2, we give some illustrations of the leaf area index evolution depending on some parameters. This new version of the model, adapted to medium resolution remote sensing images, can now be used in data assimilation schemes to combine it with images.

C. Data assimilation

Combining different sources of information driven by a physical model, commonly named "data assimilation", has always been a hot research topic for which a large panel of approaches exist. Researchers in this area have developed a number of efficient inference tools, such as stochastic methods Doucet *et al.* (2000), Kalman filter Welch and Bishop (1995) and variational approaches as the well-known 4DVAR algorithm Bain and Crisan (2009); Le Dimet and Talagrand (1986); Lions and Mitter (1971); Courtier *et al.* (1994).

In all these techniques one can model the problem as follows: the data to estimate (noted S_{t_k} at time t_k in our application), driven by a dynamical model M, are represented through a system state discretized into a sequence of hidden states Kitagawa (1996) and are observed directly or indirectly by O_{t_k} through an observation system H:

$$S_{t_{k+1}} = M_k[S_{t_k}] + \eta_{t_k} \tag{11}$$

$$O_{t_k} = H[S_{t_k}] + \epsilon_{t_k} \tag{12}$$

where η_{t_k} (resp. ϵ_{t_k}) are the system noises to estimate that models uncertainties w.r.t the dynamics M (resp. w.r.t observation operator H). In our application the prediction model M_k is based on Greenlab and is modelled in Eq. (6). As for the observation operator H, in practice because of the complexity of the relationship between the image luminance and the LAI, the definition

of a complete observation system H that directly links the LAI to data would be tricky. We therefore prefer to adopt a two stage strategy where at first we estimate the leaf area index thanks to the PROSAIL model Jacquemoud *et al.* (2009); Lecerf *et al.* (2008) and then use an identity observation operator in H. This "pseudo-observation" approach is commonly used when data assimilation systems involve complex relationships between observations and system states Courtier and Talagrand (1987). In practice, efficient tools based on neural network to inverse PROSAIL model to estimate biophysical variables from MODIS time series exist and we use the technique presented in Lecerf *et al.* (2008).

Among possible solutions mentioned above to perform model inference, variational and stochastic techniques are the most popular. Here, because of the complexity and non-linearity of our dynamical model, we prefer to rely on stochastic approaches and more precisely on the **forward-backward smoother** since we consider the whole sequence to recover all data (unlike particle filter which recovers data with the knowledge of past and current data only) Doucet (2001). Starting from:

- An observation sequence $\bar{O}_{t_k} = \{O_{t_1}, O_{t_2}..., O_{t_k}\}$ available sequentially;
- An initial distribution of the system's state $p(S_{t_1})$;
- Transition and observation models: $p(S_{t_k}|S_{t_{k-1}})$ and $p(O_{t_k}|S_{t_k})$ respectively, related to the stochastic processes M and H presented above;
- Common assumption of zero-mean time-independent Gaussian noise for η, ϵ in (11-12), leading to $p(S_{t_k}|S_{t_{k-1}}) \sim \mathcal{N}(M_k(S_{t_{k-1}}), \eta)$ and $p(O_{t_k}|S_{t_k}) \sim \mathcal{N}(H_k(S_{t_k}), \epsilon)$ with $\mathcal{N}$ the normal distribution,

it can be shown that the sequential estimation of (S_{t_k}) can be obtained using a two-fold prediction/correction system. We refer readers to Doucet (2001) for more details.

Following equations (1-6), the set of additional parameters $\{\Theta = E/r, k, \alpha, t_{e\ell}, \eta, \epsilon\}$ has to be fixed in order to describe properly the LAI evolution of a plant. Parameters E/r, k are related to environment, leaf mutual shading parameter and photosynthesis efficiency in Eq. (1), α to natural leaf foliage in Eq. (6), $t_{e\ell}$ the time expectance of leaves in (6), η to the system noise in Eq. (11) and ϵ to the observation variance in Eq. (12). They are estimated for each time step t_k by a least square between the mean state $\overline{S_{t_k}}$ of particles $S^i_{t_k}, i = \{1...N\}$ at a given time t_k and the LAI $S^e_{t_k}$ issued from GreenLab model, depending on $\{r, k, \alpha\}$ (see illustration in Fig. 2):

$$\{r, k, \alpha, t_{e\ell}\} = \arg \min_{r,k,\alpha,t_{e\ell}} \sum_{i=1}^{N} ||\overline{S_{t_k}} - S^e_{t_k}||^2. \quad (13)$$

As for the system noise η in Eq. (11), its distribution is assumed to be time independent zero-mean Gaussian. Its variance σ_η can then directly be computed in each time step t_k using available N particles with the relation:

$$\sigma_\eta = \frac{1}{N}\sum_{i=1}^{N} ||S^i_{t_k} - S^e_{t_k}||^2. \tag{14}$$

The same holds for the estimation of ϵ: noisy estimation $S^o_{t_k}$ of Leaf Area Index being acquired from each image O_{t_k} by an inversion of PROSAIL model, the uncertainty σ_ϵ related to the observation system can be extracted through:

$$\sigma_\epsilon = \frac{1}{N}\sum_{i=1}^{N} ||S^i_{t_k} - S^o_{t_k}||^2. \tag{15}$$

Concerning the initialization of the system, we estimate noisy LAI sequence $\{S^o_{t_k}|k = 1, ..., T\}$ from input images. Data with missing observations are approximated with a polynomial regression from $\{S^o_{t_k}\}$. All these steps result in the following iterative algorithm:

Incremental technique for LAI estimation and parameter inference

- Initializations:
  - From MODIS images $\{O_{t_k}\}$, compute noisy estimations $\{S^o_{t_k}\}$ of LAI folloing Lecerf *et al.* (2008);
  - Perform a polynomial regression on $\{S^o_{t_k}\}$in order to initialize $\{S^r_{t_k}|k = 1, ..., M\}$;

1) Estimate hidden parameters $\{E/r, k, \alpha, t_{e\ell}\}$ with Eq. (13)
2) Compute associated uncertainties $\{\eta, \epsilon\}$ with Eq. (14-15)
3) Perform LAI inference through particle methods described in this section (cf Doucet (2001))
4) **Loop** to step (1) until the estimation of LAI converges

- Once converged, the reconstructed Leaf Area Index sequence $\{S^r_{t_k}|k = 1, ..., M\}$ and associated hidden parameters $\Theta = \{r, k, \alpha, t_{e\ell}, \eta, \epsilon\}$ are available.

From this algorithm, we observe that the model and observation uncertainties η and ϵ are automatically adapted during the process.

III. Experimental Results

Our approach has been tested on synthetic, real data sets with ground truth and real data and in order to analyse the benefits of our method under various situations. Before entering into details, let us discuss about the experimental setup.

A. *Experimental settings*

The following experimental conditions have been applied:

- In each experiment, the number of particles has been set to 200;
- The efficiency of the reconstruction process presented in this paper has been compared with polynomial regression (5 degrees) and wavelet filter (Daubechies with 5-level). These parameters have also been set by cross-validation. When ground truth is available, only polynomial and linear interpolation has been performed since no enough data were available to test wavelet filters;
- We have indicated the results with a simulation of GreenLab with estimated parameters $(E/r, k, \alpha, t_{e\ell})$ using the proposed procedure in Section II-C. Then we could iteratively predict the LAI values without the correction steps, as demonstrated in Fig. 2. This could be considered as a model-based regression ;
- All graphes have been compensated by estimated $t_{e\ell}$ in order to have similar starting points.

B. *Data with ground truth measurements*

To evaluate the efficiency of our technique, we have used ground LAI measurements of 9 series of wheat and 9 series of rape acquired from January to July 2017 in Brittany, North France (5 ground measurements for rape and 4 ground measurements for wheat). These measurements act as ground truth validation. All series have been acquired on different parcels (whose size are larger than one SENTINEL-2 pixel) to sense the variability of our approach. Investigated areas are part of a Long Ecological Research site named "Pleine Fougres", located on the southern part of the Bay of Mont-Saint-Michel, France, and referenced in the LTER-Europe[1] and ILTER networks[2]. This agricultural landscape is dominated by fields of wheat, maize, rapeseed and grasslands. Field observations and measurements were conducted on the study site during one crop year (2017) in order to calibrate and quantitatively validate the proposed approach. Different parameters were measured and georeferenced once per three weeks using a GPS (5 m accuracy): water saturation, vegetation height and LAI, whereas phenology stages, dates of sowing and harvests, and yields were observed in 18 fields.

[1]See: http://www.lter-europe.net/

[2]See: https://www.ilter.network/

An illustration of the position of on site measurements is visible in figure 4. Corresponding SENTINEL-2 images (9 images during the period) have been downloaded and our process has been applied on pixels associated with parcels. To evaluate the efficiency of the GreenLab model, data from May to September (resp. from February to May) have been removed in the processing of wheat (resp. rape). This choice has been done on the basis of the associated phenological states in order to remove from observations the main informations. Estimated values (one image per day) have been compared with ground truth.

Associated errors (mean and standard deviations on 100 realisations) and illustrations of some reconstructions are respectively depicted on table I and figure 5 both for wheat and rape. As one can observe on figure 5, the assimilations with GreenLab (particle filter and smoother) are systematically more in accordance with ground truth than interpolations. For example in all series with wheat, as the maximum of LAI is never observed, interpolation techniques that are not driven by a physical model fail in recovering the growth and decrease of LAI. On the contrary, the use of a physical model enables to better recover the physical evolution of LAI. The same kind of observations stands for rape. Here, as observations during the growing period are missing (from February to May), interpolation techniques fail in recovering the variability of the growth, unlike our assimilation approach. All these observations can be confirmed with quantitative values in table I where assimilations with particle smoother (and then filter) systematically outperform interpolation techniques.

These first experiments with ground truth measurements confirm the ability of our technique to recover LAI thanks to the GreenLab model. We now turn to experiments with estimated LAI.

C. Data with estimated LAI

Data used are issued from real MODIS reflectance product (a sequence of 17 images) on which LAI estimations, issued from the PROSAIL model, have been reconstructed and validated (see Lecerf *et al.* (2008, 2005)). In addition, associated classifications of large agricultural parcels (we mean by *large* the fact that they recover more than one MODIS pixel) were available, providing us confident LAI time series and associated land cover. In practice three types of agricultural crops were used: colza, maize and wheat. Some LAI profiles are visible in Fig. 3.

To model the various artefacts prone to occur in remote sensing images, several processes have been applied on these data:

- *Noisy observations.* Data are equally subsampled (one image every 10 days) from ground data and a Gaussian white noise has been introduced as shown in Fig. 6.
- *Sparse observations.* Data for only 6 observations have been kept. The motivation is to evaluate the performance of our algorithm under a short length of remote sensing observation time series (very cloudy regions), as shown in Fig. 7.
- *Missing observations.* Very few observations were used (7 in practice) but here we simulate the absence of data during a long series. Therefore missing data are consecutive in time as shown in Fig. 8.

1) Result on sequence of noisy observations: This kind of data represents a great challenge in remote sensing analysis since all observations are in general corrupted by noise and conventional techniques often require to have an estimation of such noise Rabiner and Gold (1975); Burrus *et al.* (1998), unlike our process.

In order to make a quantitative evaluation, various levels of Gaussian zero-mean noise, with Signal-to-noise ratio (SNR) ranging from 2 to 10, were tested. The table II represents the root-mean-square error (RMSE) between reconstructed LAI (with particle filter and smoother and other reconstruction techniques introduced in section III-A) and reference data for 100 realizations. It is interesting to observe in this table that the introduction of GreenLab plant growth model in the reconstruction process systematically reduces the error residual and outperforms all other methods. Particles smoother almost always gives a better performance than particle filter, which is quite rational as when estimating the LAI at any time point, particle filter only exploits information of up-to-date observations, while particle smoother takes into account all observations in time series. In order to have a visual inspection of the reconstructions, some illustrations are visible in Fig. 6 and confirm that our outputs are of reliable quality. Even if other curves are sometimes consistent with ground truth, particle filter and/or smoother represent the best compromise since strong errors are likely to appear with other techniques (as the polynomial one very sensible to little variations).

2) Sequence with sparse observations: We have randomly taken only six observations to reconstruct the whole time series. These observations are represented by blue dotted points in Fig. 7. As one can observe, they are more or less issued from a uniform sample along the time period. Quantitative results are depicted in table III. Here again, the performance and the benefit of relying on GreenLab growth model is illustrated. Reconstructed curves are also visible in figure 7 and demonstrate the great ability of our technique to recover proper series.

3) Sequence of missing observations: We have removed long periods of consecutive data. Some illustrations are visible in Fig. 8 where one can observe that no observations during the growing period are available, which is a very delicate problem. Despite these difficulties, the proposed framework is able to provide very good reconstruction of LAI time series, as shown in Tab. IV and in Fig. 8. Obviously here, only the dynamical model prior is able to estimate consistent values during critical periods of missing data. This is to our opinion a very interesting behaviour of our estimators.

In this three experiments, various reconstruction methods have been tested. In all situations, the use of GreenLab as prior plant growth model has enabled to improve the reconstruction of LAI over long time periods. This is to our opinion a very interesting behavior likely to have many potential applications. It should also be outlined that our technique not only reconstructs the LAI but is also able to extract deviations with respect to observations and dynamical model (parameters $\{\eta, \epsilon\}$) and internal parameters of plants $\{E/r, k, \alpha, t_{e\ell}\}$. This point may have interesting applications in the future. At the moment, three species (wheat, rape, maize) have been studied but the functional part of GreenLab enables this model to adapt to many other kind of cultures. Associated landscapes (Brittany, France) and crops on which our experimentations have been performed are very fragmented, which disturbs the observation with moderate remote sensing images. It is expected that in larger areas (USA, China, ...), the application of our process would be easier. It is also important to point out that some recent domain adaptation techniques Courty *et al.* (2017) issued from machine learning and artificial intelligence (how to fit a model designed for one site to another site) could be tested on these assimilation approaches to adapt this work to other regions or species. This is actually the scope of a current work.

This second series of experiments has quantitatively demonstrated the efficiency of our technique. Let us now present experiments on real MODIS data.

D. Application on large scale study site

We have applied our methods on a large scale study site in Chizé, France. This study site is abundant with various sorts of vegetation, such as wood, grassland, maize, colza, wheat. In practice 16 images from March to October 2006 were available. On these images, the PROSAIL model has been applied to derive LAI time series. An illustration of available data is visible in the top of Fig. 11 where red stands for high values of LAI (indicating dense plant canopy) and

blue for low LAI. However at some location, observation data are corrupted, mainly because of cloud coverage, yielding corrupted time series.

In the bottom of figure 11, the results from particle smoother under our proposed framework are depicted. In addition we have plotted in Fig. 9 some curves randomly taken from the images. Despite the fact that no ground truth exist here, it appears obviously that our method seems consistent and enables to recover uncorrupted LAI time series.

IV. Conclusion

In this paper, we have proposed a technique that estimates leaf area index time series using data assimilation. The dynamical model is based on the GreenLab plant growth model where a number of modifications have been applied to adapt it in a remote sensing context. LAI observations are issued from the inversion of the PROSAIL model. As shown in our experiments, this technique is efficient in many various situations as very sparse observations or missing/noisy data. Quantitatively, it outperforms other reconstruction strategies that do not rely on a physical prior knowledge, especially when large period of missing data occur. An additional key point of our process is its ability to estimate internal parameters of the plant unobservable from images (environmental parameters, spoilage, ...). This is to our opinion a very good property that open new applications in the future.

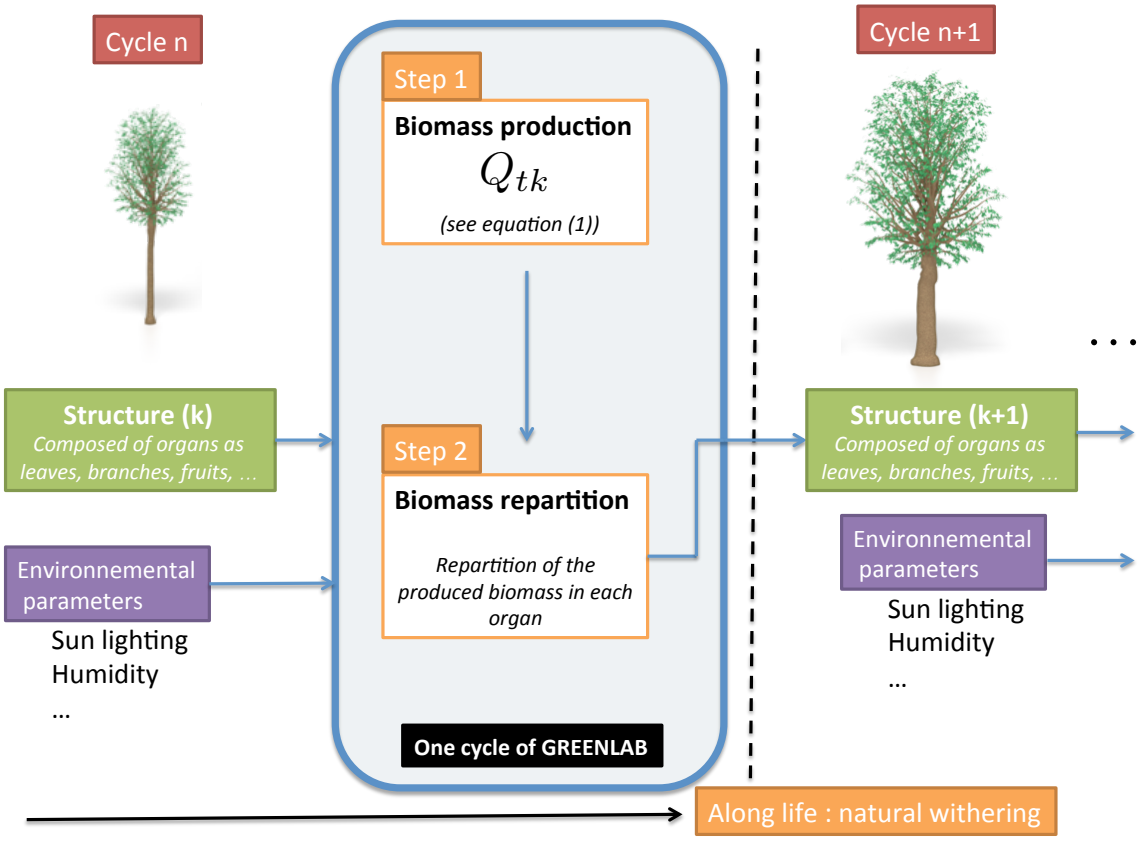

Fig. 1. **Illustration of GreenLab model with two steps:** in each cycle, the **biomass production** step computes the produced biomass based on the current plant structure and environmental parameters. The **biomass repartition** step allocates this biomass in various organs to generate a new plant at cycle $n+1$. All these operations are balanced by healthy coefficients that model the **natural withering**

424

425

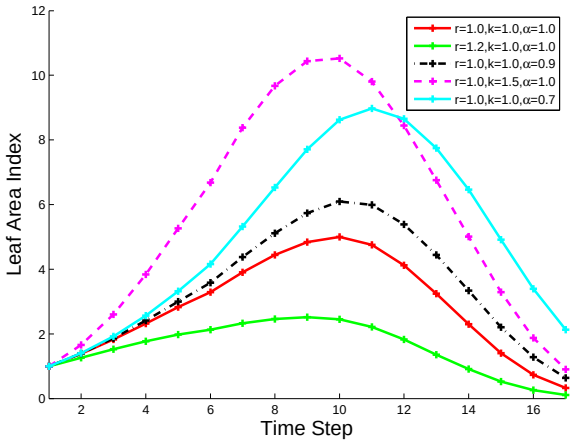

Fig. 2. **Leaf area index evolution with different** r, k, α

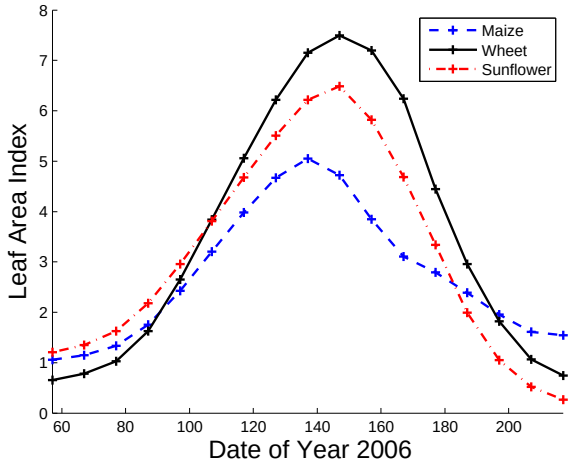

Fig. 3. A demonstration of uncorrupted LAI time series for three sorts of agriculture crops in Brittany, France

Fig. 4. **Localisation of on site measurements** for wheat and rape in Brittany, North of France. All parcels are higher than a SENTINEL-2 pixel area

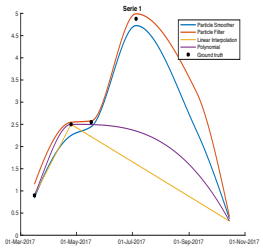

(a): wheat serie #1

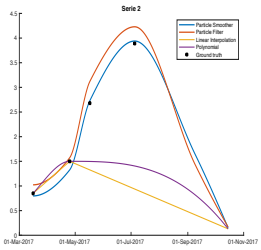

(b): wheat serie #2

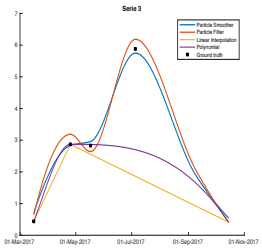

(c): wheat serie #3

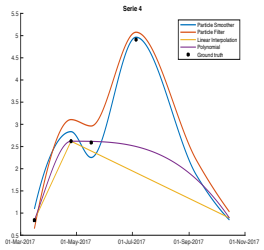

(d): wheat serie #4

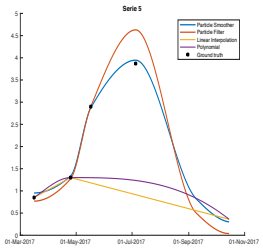

(e): wheat serie #5

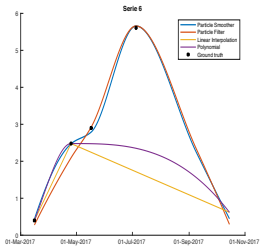

(f): wheat serie #6

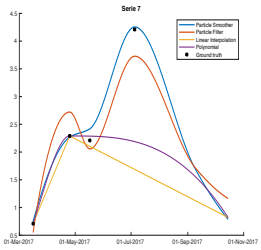

(g): wheat serie #7

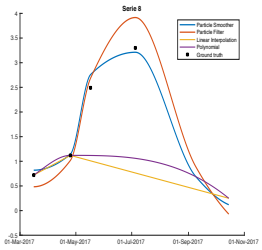

(h): wheat serie #8

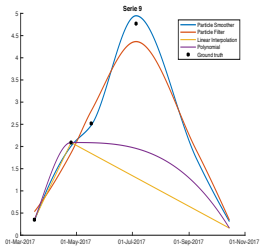

(i): wheat serie #9

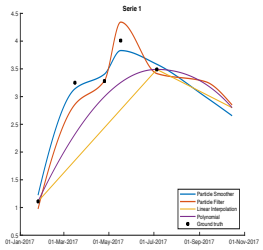

(j): rape serie #1

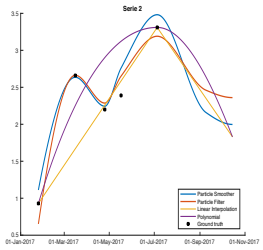

(k): rape serie #2

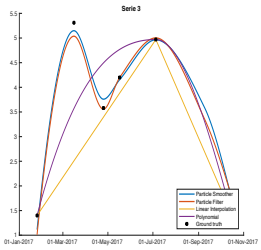

(l): rape serie #3

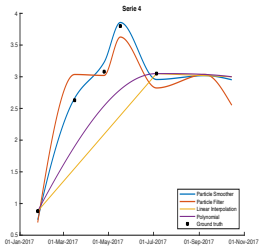

(m): rape serie #4

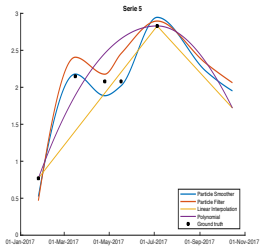

(n): rape serie #5

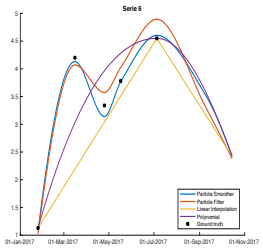

(o): rape serie #6

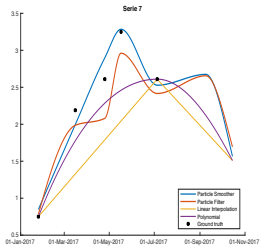

(p): rape serie #7

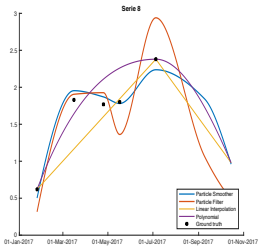

(q): rape serie #8

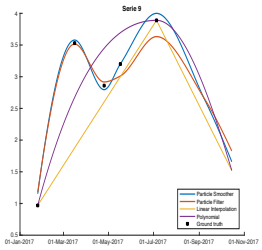

(r): rape serie #9

Fig. 5. **LAI reconstruction for wheat and rape with ground truth superposition** over the year 2017 with missing data from May to September (wheat) and from February to May (rape). Ground truth measurements are block dots, GreenLab assimilation with particle smoother (our technique) is in blue, GreenLab assimilation with particle filter is in red, polynomial interpolation in purple and linear interpolation in yellow.

TABLE I

ROOT-MEAN-SQUARE ERROR (RMSE) IN RECOVERING LAI FOR ALL SERIES AND IN AVERAGE FOR WHEAT (TOP) AND RAPE (BOTTON).

Wheat Series #	Polynomial	Linear	Particle Filter	Particle Smoother
1	1.2656	1.6455	0.2904±0.1056	**0.1447±0.0557**
2	1.3759	1.6240	0.2722±0.0996	**0.1354±0.0541**
3	1.5901	2.0144	0.2765±0.1175	**0.1419±0.0501**
4	1.2049	1.5030	0.2978±0.1117	**0.1420±0.0453**
5	1.5419	1.7098	0.2948±0.1103	**0.1450±0.0540**
6	1.6430	1.9742	0.2861±0.1021	**0.1458±0.0546**
7	1.0115	1.2628	0.2861±0.1047	**0.1416±0.0427**
8	1.3134	1.4688	0.2821±0.0976	**0.1415±0.0565**
9	1.4233	1.7686	0.2912±0.0944	**0.1434±0.0529**
Average	1.3744	1.6634	0.2864±0.1048	**0.1424±0.0518**
Rape Series #	Polynomial	Linear	Particle Filter	Particle Smoother
1	0.3870	0.4039	0.2934±0.1000	**0.1442±0.0529**
2	0.2488	0.2025	0.2767±0.1042	**0.1359±0.0488**
3	0.9274	0.6938	0.2729±0.0961	**0.1408±0.0470**
4	0.4925	0.5515	0.2909±0.1059	**0.1466±0.0524**
5	0.0464	0.0354	0.2814±0.0951	**0.1384±0.0497**
6	0.4558	0.3834	0.2835±0.1046	**0.1546±0.0484**
7	0.4504	0.5028	0.2669±0.0996	**0.1431±0.0501**
8	0.0296	0.0175	0.3003±0.1124	**0.1443±0.0501**
9	0.3396	0.2485	0.2917±0.1107	**0.1432±0.0565**
Average	0.3753	0.3377	0.2842±0.1032	**0.1435±0.0507**

TABLE II

THE ROOT-MEAN-SQUARE ERROR (RMSE) OF DIFFERENT METHODS ON SEQUENCES OF VARIOUS SNR LEVEL.

RMSE	SNR=2	SNR=4	SNR=6	SNR=8	SNR=10
Observations	1.3222±0.2637	0.8712±0.1712	0.7747±0.1327	0.6707±0.1300	0.6313±0.0895
Polynomial	0.7971±0.2126	0.6120±0.1535	0.5760±0.1168	0.5351±0.0893	0.5136±0.0770
Wavelet filter	0.8018±0.1749	0.7040±0.0895	0.6795±0.0793	0.6481±0.0848	0.6365±0.0548
Fitted model	**0.7063±0.2477**	0.5749±0.1829	0.5259±0.1561	0.5189±0.1699	0.4586±0.0843
Particle filter	0.7755±0.2500	0.6633±0.1822	0.5973±0.1329	0.5452±0.1327	0.5403±0.1175
Particle smoother	0.7072±0.2495	**0.5660±0.1634**	**0.5014±0.1240**	**0.4837±0.1036**	**0.4341±0.1057**

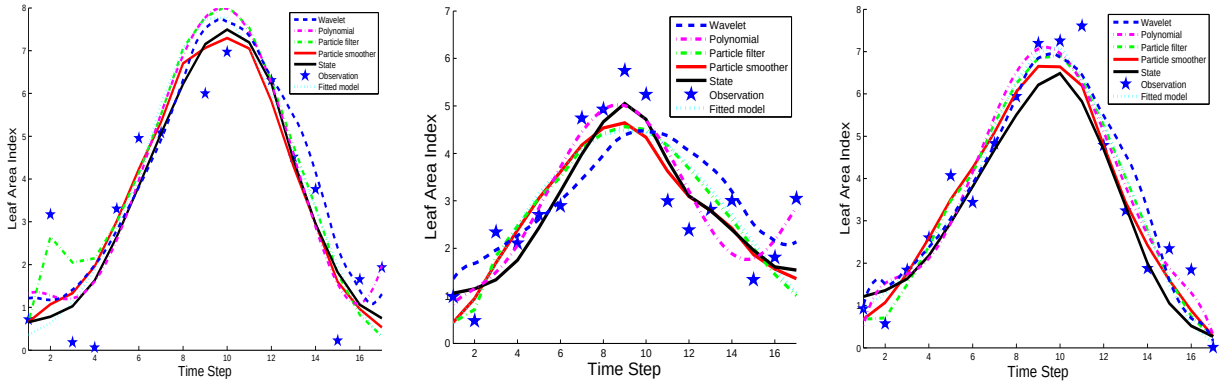

(a)Wheat (b)Maize (c)Colza

Fig. 6. **LAI reconstruction with various techniques on the sequence of noisy observations (with SNR=6).** Dark line are uncorrupted MODIS observations (ground truth state), blue dots are the input noisy observations, red line is the result of reconstruction with particle smoother, cyan line from particle filter, green line from fitted model, pink line from polynomial regression, blue line from wavelet filter. Even in this situation where the noise is large, the best fitted curves are issued from techniques based on the GreenLab model

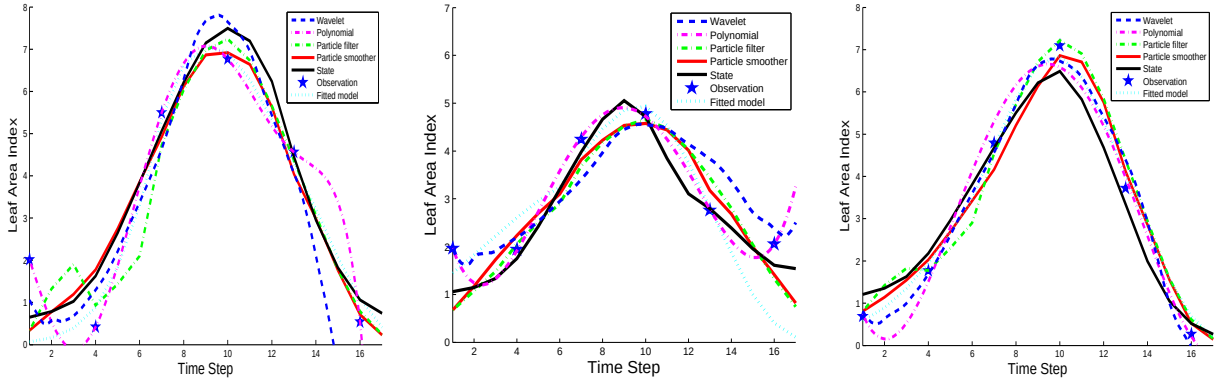

(a)Wheat (b)Maize (c)Colza

Fig. 7. **LAI reconstruction with various techniques on the sequence of sparse observations (with SNR=6).** Dark line are uncorrupted MODIS observations (ground truth state), blue dots are the input noisy observations, red line is the result of reconstruction with particle smoother, cyan line from particle filter, green line from fitted model, pink line from polynomial regression, blue line from wavelet filter.

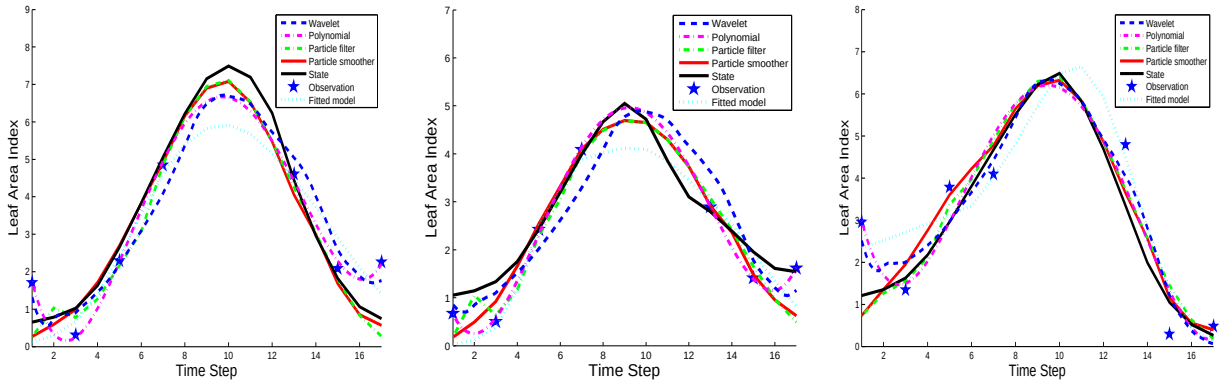

(a)Wheat (b)Maize (c)Colza

Fig. 8. **LAI reconstruction with various techniques on the sequence of missing observations (with SNR=6) .** Dark line are uncorrupted MODIS observations (ground truth state), blue dots are the input noisy observations, red line is the result of reconstruction with particle smoother, cyan line from particle filter, green line from fitted model, pink line from polynomial regression, blue line from wavelet filter.

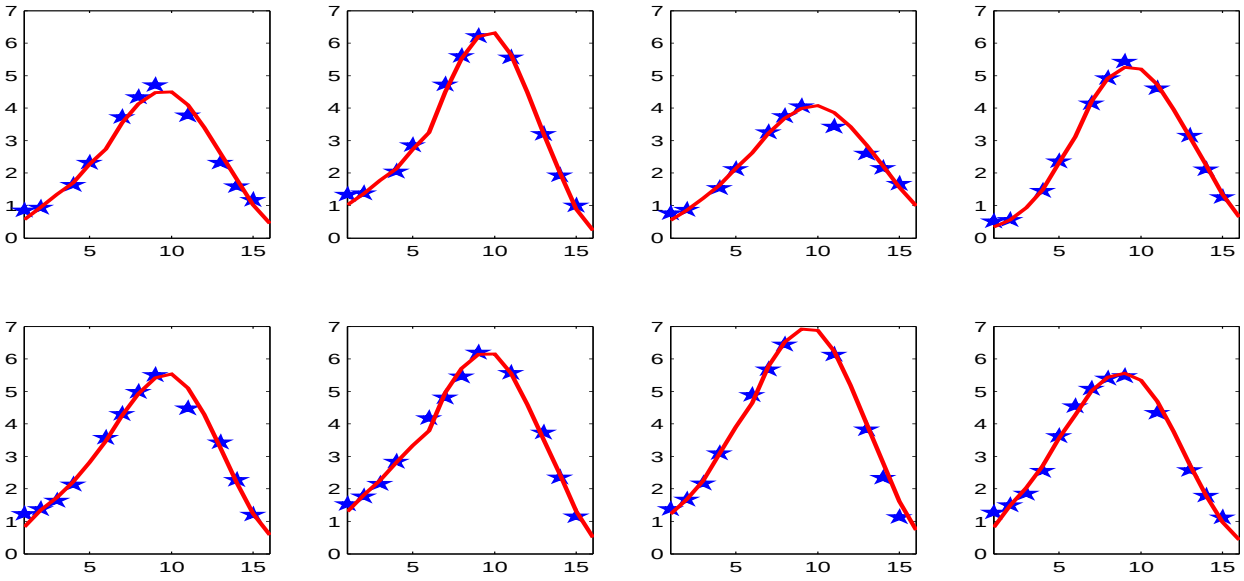

Fig. 9. **Several examples of LAI time series reconstruction with particle smoother at a study site in Chizé, France**

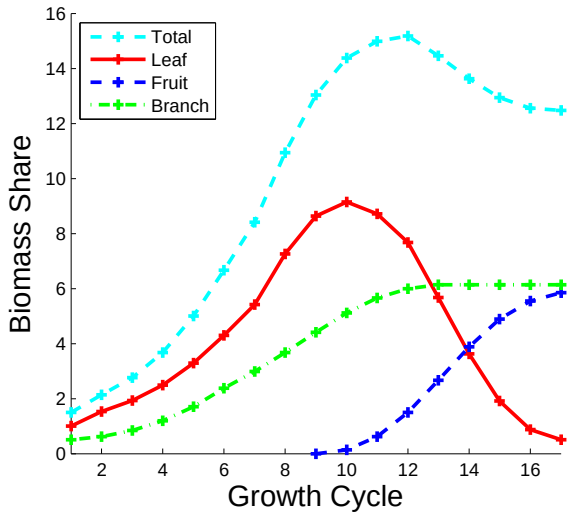

Fig. 10. **Estimated biomass production and its partition during continuous growth cycles of unit wheat field.**

TABLE III

THE ROOT-MEAN-SQUARE ERROR (RMSE) OF DIFFERENT METHODS ON SEQUENCE WITH SPARSE OBSERVATIONS.

RMSE	SNR=2	SNR=4	SNR=6	SNR=8	SNR=10
Observations	1.4425±0.3580	1.2365±0.3881	0.9455±0.3495	0.7818±0.2562	0.6887±0.1431
Polynomial	1.4943±0.5823	1.2852±0.1447	0.1447±0.4577	0.8807±0.3098	0.7867±0.1761
Wavelet filter	1.1932±0.4386	1.1424±0.3814	1.0390± 0.4995	0.7390±0.2517	0.7229±0.1860
Fitted model	1.0346±0.3362	1.0425±0.3267	0.8574±0.3565	0.6767±0.3192	0.7126±0.2611
Particle filter	1.1762±0.3986	1.1233±0.3220	0.8523±0.3780	0.7931±0.3361	0.7549±0.1903
Particle smoother	**1.0198±0.3526**	**0.9622±0.3477**	**0.9451±0.3330**	**0.5923±0.2364**	**0.5919±0.1420**

TABLE IV

THE ROOT-MEAN-SQUARE ERROR (RMSE) OF DIFFERENT METHODS ON SEQUENCE OF MISSING OBSERVATIONS.

RMSE	SNR=2	SNR=4	SNR=6	SNR=8	SNR=10
Observations	1.2934±0.3317	1.0424±0.2523	0.9218±0.2468	0.7011±0.1642	0.7118±0.1709
Polynomial	1.2606±0.5608	1.1733±0.4756	1.0649±0.4444	1.1239±0.6996	0.8877±0.5777
Wavelet filter	1.3656±0.6070	1.0531±0.3697	0.8184± 0.2907	0.7741±0.3403	0.7840±0.3407
Fitted model	**1.2036±0.6758**	1.0689±0.4229	0.8079±0.2906	0.7072±0.3583	0.6894±0.3031
Particle filter	1.2617±0.6158	0.9596±0.3778	0.8526±0.2759	0.7232±0.3553	0.7044±0.3254
Particle smoother	1.2065±0.6876	**1.0253±0.4510**	**0.8055±0.3180**	**0.7050±0.3578**	**0.6892±0.3479**

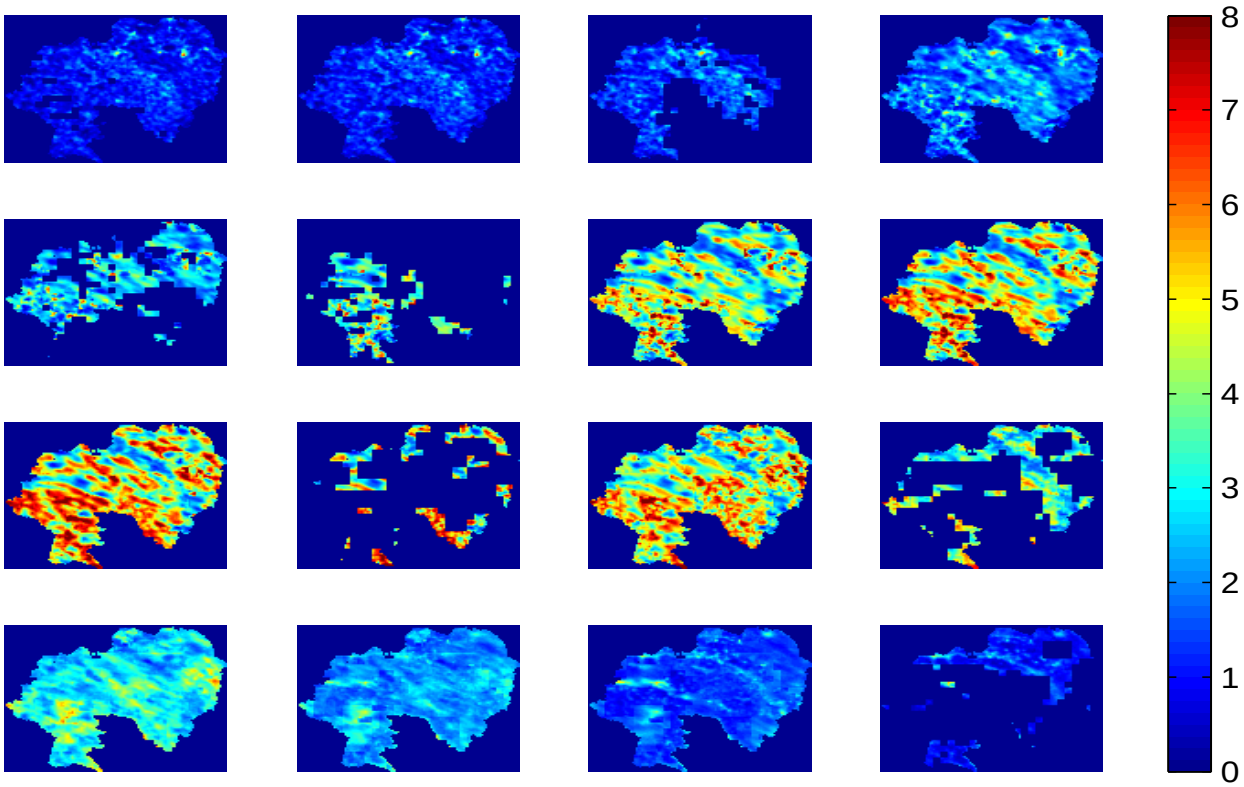

(a)

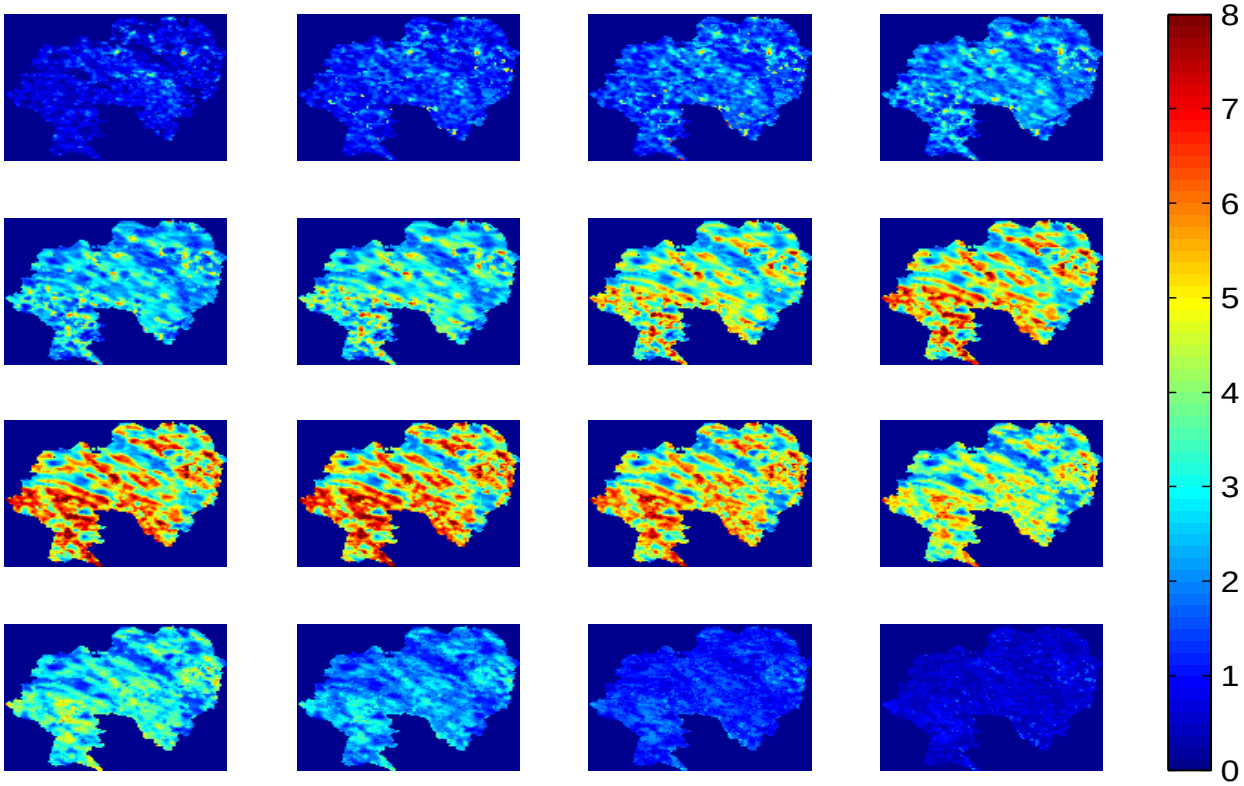

(b)

Fig. 11. **Result of particle smoother at a study site in Chizé, France**

426 ## REFERENCES

427 Bain, A. and Crisan, D. (2009). *Fundamentals of stochastic filtering*, volume 3. Springer.

428 Baret, F., Hagolle, O., Geiger, B., Bicheron, P., Miras, B., Huc, M., Berthelot, B., Niño, F.,
429 Weiss, M., Samain, O., *et al.* (2007). Lai, fapar and fcover cyclopes global products derived
430 from vegetation: Part 1: Principles of the algorithm. *Remote sensing of environment*, **110**(3),
431 275–286.

432 Brisson, N., Gary, C., Justes, E., Roche, R., Mary, B., Ripoche, D., Zimmer, D., Sierra, J.,
433 Bertuzzi, P., Burger, P., *et al.* (2003). An overview of the crop model stics. *European Journal*
434 *of agronomy*, **18**(3), 309–332.

435 Burrus, C. S., Gopinath, R. A., Guo, H., Odegard, J. E., and Selesnick, I. W. (1998). *Introduction*
436 *to wavelets and wavelet transforms: a primer*, volume 23. Prentice hall Upper Saddle River.

437 Carlson, T. N. and Ripley, D. A. (1997). On the relation between ndvi, fractional vegetation
438 cover, and leaf area index. *Remote sensing of Environment*, **62**(3), 241–252.

439 Cohen, D. (1967). Computer simulation of biological pattern generation processes. *Nature*,
440 **216**(5112), 246–248.

441 Courtier, P. and Talagrand, O. (1987). Variational assimilation of meteorological observations
442 with the adjoint vorticity equation. ii: Numerical results. *Quarterly Journal of the Royal*
443 *Meteorological Society*, **113**(478), 1329–1347.

444 Courtier, P., Thépaut, J.-N., and Hollingsworth, A. (1994). A strategy for operational implemen-
445 tation of 4d-var, using an incremental approach. *Quarterly Journal of the Royal Meteorological*
446 *Society*, **120**(519), 1367–1387.

447 Courty, N., Flamary, R., Tuia, D., and Rakotomamonjy, A. (2017). Optimal transport for domain
448 adaptation. *IEEE transactions on pattern analysis and machine intelligence*, **39**(9), 1853–1865.

449 Curnel, Y., de Wit, A. J., Duveiller, G., and Defourny, P. (2011). Potential performances of
450 remotely sensed lai assimilation in wofost model based on an oss experiment. *Agricultural*
451 *and Forest Meteorology*, **151**(12), 1843–1855.

452 Dayan, E., Presnov, E., and Fuchs, M. (2004). Prediction and calculation of morphological
453 characteristics and distribution of assimilates in the rosgro model. *Mathematics and Computers*
454 *in Simulation*, **65**(1-2), 101–116.

455 De Reffye, P., Fourcaud, T., Blaise, F., Barthélémy, D., and Houllier, F. (1997). A functional
456 model of tree growth and tree architecture.

457 Dente, L., Satalino, G., Mattia, F., and Rinaldi, M. (2008). Assimilation of leaf area index
458 derived from asar and meris data into ceres-wheat model to map wheat yield. *Remote sensing*
459 *of Environment*, **112**(4), 1395–1407.

460 Doucet, A. (2001). *Sequential monte carlo methods*. Wiley Online Library.

461 Doucet, A., Godsill, S., and Andrieu, C. (2000). On sequential monte carlo sampling methods
462 for bayesian filtering. *STATISTICS AND COMPUTING*, **10**(3), 197–208.

463 Fisher, J. (1992). How predictive are computer simulations of tree architecture? *International*
464 *Journal of Plant Sciences*, **153**(3, Part 2), S137–S146.

465 Gamon, J. A., Field, C. B., Goulden, M. L., Griffin, K. L., Hartley, A. E., Joel, G., Peñuelas, J.,
466 and Valentini, R. (1995). Relationships between ndvi, canopy structure, and photosynthesis
467 in three californian vegetation types. *Ecological Applications*, pages 28–41.

468 Gao, B.-C. (1996). Ndwiła normalized difference water index for remote sensing of vegetation
469 liquid water from space. *Remote sensing of environment*, **58**(3), 257–266.

470 González-Sanpedro, M., Le Toan, T., Moreno, J., Kergoat, L., and Rubio, E. (2008). Seasonal
471 variations of leaf area index of agricultural fields retrieved from landsat data. *Remote Sensing*
472 *of Environment*, **112**(3), 810–824.

473 Guo, Y., Ma, Y.-T., Zhan, Z.-G., Li, B.-G., Dingkuhn, M., Luquet, D., and De Reffye, P. (2006).
474 Parameter optimization and field validation of the functional–structural model greenlab for
475 maize. *Annals of Botany*, **97**(2), 217–230.

476 Heuvelink, E. (1999). Evaluation of a dynamic simulation model for tomato crop growth and
477 development. *Annals of Botany*, **83**(4), 413–422.

478 Honda, H. (1971). Description of the form of trees by the parameters of the tree-like body:
479 Effects of the branching angle and the branch length on the shape of the tree-like body.
480 *Journal of theoretical biology*, **31**(2), 331–338.

481 Huete, A. R. (1988). A soil-adjusted vegetation index (savi). *Remote sensing of environment*,
482 **25**(3), 295–309.

483 Jacquemoud, S., Verhoef, W., Baret, F., Bacour, C., Zarco-Tejada, P. J., Asner, G. P., François, C.,
484 and Ustin, S. L. (2009). Prospect+ sail models: A review of use for vegetation characterization.
485 *Remote Sensing of Environment*, **113**, S56–S66.

486 Jallas, E., Martin, P., Sequeira, R., Turner, S., Cretenet, M., and Gérardeaux, E. (2000). Virtual
487 cotons®, the firstborn of the next generation of simulation model. In *Virtual Worlds*, pages
488 235–244. Springer.

Jonsson, P. and Eklundh, L. (2002). Seasonality extraction by function fitting to time-series of satellite sensor data. *Geoscience and Remote Sensing, IEEE Transactions on*, **40**(8), 1824–1832.

Kang, M.-Z., Cournède, P.-H., De Reffye, P., Auclair, D., and Hu, B.-G. (2008). Analytical study of a stochastic plant growth model: application to the greenlab model. *Mathematics and Computers in Simulation*, **78**(1), 57–75.

Kitagawa, G. (1996). Monte carlo filter and smoother for non-gaussian nonlinear state space models. *Journal of computational and graphical statistics*, **5**(1), 1–25.

Kurth, W. and Sloboda, B. (1997). Growth grammars simulating trees–an extension of l-systems incorporating local variables and sensitivity.

Launay, M. and Guerif, M. (2005). Assimilating remote sensing data into a crop model to improve predictive performance for spatial applications. *Agriculture, ecosystems & environment*, **111**(1-4), 321–339.

Le Dimet, F. and Talagrand, O. (1986). Variational algorithms for analysis and assimilation of meteorological observations: theoretical aspects. *Tellus A*, **38**(2), 97–110.

Lecerf, R., Corpetti, T., Hubert-Moy, L., and Dubreuil, V. (2005). Monitoring land use and land cover changes in oceanic and fragmented landscapes with reconstructed modis time series. In *Third International Workshop on the Analysis of Multi-temporal Remote Sensing Images, Multitemp*, pages 195–199, Biloxi, Mississippi USA.

Lecerf, R., Hubert-Moy, L., Corpetti, T., Baret, F., Latif, B. A., and Nicolas, H. (2008). Estimating biophysical variables at 250 m with reconstructed eos/modis time series to monitor fragmented landscapes. In *Geoscience and Remote Sensing Symposium, 2008. IGARSS 2008. IEEE International*, volume 2, pages II–954. IEEE.

Liang, S. (2005). *Quantitative remote sensing of land surfaces*, volume 30. John Wiley & Sons.

Lindenmayer, A. (1968). Mathematical models for cellular interactions in development i. filaments with one-sided inputs. *Journal of theoretical biology*, **18**(3), 280–299.

Lions, J. L. and Mitter, S. K. (1971). *Optimal control of systems governed by partial differential equations*, volume 1200. Springer Berlin.

Lopez, G., Favreau, R. R., Smith, C., Costes, E., Prusinkiewicz, P., and DeJong, T. M. (2008). Integrating simulation of architectural development and source–sink behaviour of peach trees by incorporating markov chains and physiological organ function submodels into l-peach. *Functional Plant Biology*, **35**(10), 761–771.

Ma, Y., Wen, M., Li, B., Guo, Y., Cournede, P.-H., and De Reffye, P. (2006). Calibration of greenlab model for maize with sparse experimental data. In *Plant Growth Modeling and Applications, 2006. PMA'06. Second International Symposium on*, pages 188–193. IEEE.

Mathieu, A., Zhang, B., Heuvelink, E., Liu, S., Cournède, P.-H., and de Reffye, P. (2007). Calibration of fruit cyclic patterns in cucumber plants as a function of source-sink ratio with the greenlab model. In *Proceedings of the 5th International Workshop om Functional-Structural Plant Models, Napier, New Zealand, 4-9 November, 2007*, pages 1–5.

Perttunen, J., ÄNEN, R. S., Nikinmaa, E., Salminen, H., Saarenmaa, H., *et al.* (1996). Lignum: a tree model based on simple structural units. *Annals of Botany*, **77**(1), 87–98.

Przemyslaw, P., Prusinkiewicz, P., Lindenmayer, A., and Hanan, J. (1988). Developmental models of herbaceous plants for computer imagery purposes. *Computer Graphics*, **22**(4).

Rabiner, L. R. and Gold, B. (1975). Theory and application of digital signal processing. *Englewood Cliffs, NJ, Prentice-Hall, Inc., 1975. 777 p.*, **1**.

Reeves, W. T. and Blau, R. (1985). Approximate and probabilistic algorithms for shading and rendering structured particle systems. In *ACM Siggraph Computer Graphics*, volume 19, pages 313–322. ACM.

Richards, J. A. (2013). *Remote sensing digital image analysis: an introduction*. Springer.

Roerink, G., Menenti, M., and Verhoef, W. (2000). Reconstructing cloudfree ndvi composites using fourier analysis of time series. *International Journal of Remote Sensing*, **21**(9), 1911–1917.

Rouse Jr, J., Haas, R., Schell, J., and Deering, D. (1974). Monitoring vegetation systems in the great plains with erts.

Schaepman-Strub, G., Schaepman, M., Painter, T., Dangel, S., and Martonchik, J. (2006). Reflectance quantities in optical remote sensingłdefinitions and case studies. *Remote sensing of environment*, **103**(1), 27–42.

Smith, A. (1984). Plants, fractals, and formal languages. *ACM SIGGRAPH Computer Graphics*, **18**(3), 1–10.

Townshend, J., Justice, C., Li, W., Gurney, C., and McManus, J. (1991). Global land cover classification by remote sensing: present capabilities and future possibilities. *Remote Sensing of Environment*, **35**(2), 243–255.

Trotter, C. M. (1991). Remotely-sensed data as an information source for geographical information systems in natural resource management a review. *International Journal of*

Geographical Information System, **5**(2), 225–239.

Verhoef, W. (1984). Light scattering by leaf layers with application to canopy reflectance modeling: the sail model. *Remote sensing of environment*, **16**(2), 125–141.

Viennot, X., Eyrolles, G., Janey, N., and Arques, D. (1989). Combinatorial analysis of ramified patterns and computer imagery of trees. In *ACM SIGGRAPH Computer Graphics*, volume 23, pages 31–40. ACM.

Vos, J., Marcelis, L., and Evers, J. (2007). Functional-structural plant modelling in crop production: adding a dimension. *Frontis*, pages 1–12.

Wang, F., Kang, M., Lu, Q., Han, H., Letort, V., Guo, Y., De Reffye, P., and Li, B. (2009). Calibration of topological development in the procedure of parametric identification: application of the stochastic greenlab model for pinus sylvestris var. mongolica. In *Plant Growth Modeling, Simulation, Visualization and Applications (PMA), 2009 Third International Symposium on*, pages 26–33. IEEE.

Wang, F., Kang, M., Lu, Q., Letort, V., Han, H., Guo, Y., de Reffye, P., and Li, B. (2011). A stochastic model of tree architecture and biomass partitioning: application to mongolian scots pines. *Annals of Botany*, **107**(5), 781–792.

Welch, G. and Bishop, G. (1995). An introduction to the kalman filter.

Yan, H.-P., Kang, M.-Z., De Reffye, P., and Dingkuhn, M. (2004). A dynamic, architectural plant model simulating resource-dependent growth. *Annals of Botany*, **93**(5), 591–602.

Yang, S.-H., Hu, B.-G., and Cournède, P.-H. (2008). Structural identifiability of generalized constraint neural network models for nonlinear regression. *Neurocomputing*, **72**(1), 392–400.

Zhao, Y., Chen, S., and Shen, S. (2013). Assimilating remote sensing information with crop model using ensemble kalman filter for improving lai monitoring and yield estimation. *Ecological modelling*, **270**, 30–42.